Impinging jet passive control fo wall shear stress enhancement

K. Sodjavi, B. Montagné, Magdalena Kristiawan, Amina Meslem, I. Nastase

Proceedings of the 15th International Heat Transfer Conference, IHTC-15
August 10-15, 2014, Kyoto, Japan

IHTC15-□□□□□

IMPINGING JET PASSIVE CONTROL FOR WALL SHEAR STRESS ENHANCEMENT

K. Sodjavi[1*], B. Montagné[1], A. Meslem[1], M. Kristiawan[2], I. Nastase[3]

[1]LaSIE, University of La Rochelle, Pôle Sciences et Technologie, Avenue Michel Crépeau, 17042 La Rochelle, France
[2]Institut National de la Recherche Agronomique, BIA, BP 71627, 44316 Nantes, France
[3]CAMBI Research Center, Technical University of Civil Engineering in Bucharest, Building Services Faculty, Avenue Pache Protopescu 66, Bucharest, Romania

ABSTRACT

Heat, mass and momentum transfer induced on a wall by an impinging jet are linked to vortices organization at the jet exit, themselves influenced by jet nozzle geometry. Particle Image Velocimetry (PIV) and electrodiffusion techniques were used to investigate the characteristics of three impinging jets. Two cruciform jets, one issuing from a plane orifice nozzle (CO/P) and the second from a hemispherical orifice nozzle (CO/H), were compared to a reference round jet issuing from a convergent nozzle. The distance between the jet exit and the target wall is equal to 2 nozzle equivalent diameters (D_e). The Reynolds number based on D_e and on the exit bulk-velocity was equal to 5290 in each flow. The analysis of mean and fluctuating flow fields from PIV enables the identification of flows characteristics. The jet spreading rate and the turbulence intensities before impingement were found to be higher in the jet issuing from CO/H nozzle. The switching-over phenomena observed in CO/P nozzle jet does not occur in CO/H nozzle jet. Electrodiffusion measurements reveal some differences in the shape and the level of radial distributions of wall shear rates. Of the most important observations is the large difference between the three jets in the wall shear stress levels. For the same exit bulk-velocity, the maximum wall shear rate in CO/P and CO/H nozzle jets are almost two and three times respectively higher than the one of the reference convergent jet.

KEY WORDS: Impinging jet, lobed jet, PIV, Electrodiffusion, wall shear rate

1. INTRODUCTION

In the field of fundamental and applicative researches on turbulent jets, it was observed many times, as in [1-4], that the characteristics of initial shear layer and of the subsequent vortices which are forming in the jet near field, are directly related to the inlet conditions governed by an intentional and/or an accidental excitations of the shear layer. Intentional alteration of the initial conditions by active [5, 6] or passive [7-9] techniques causes considerable modification of the large-scale vortices in both their shape and convection velocities. Those techniques are commonly used to improve jet self-induction which is useful in mixing processes as in combustion chambers. The influence of initial conditions on jet dynamics is attributed to the underlying structure of turbulent motions that is carried from the jet inlet throughout the flow field. A thorough research (beginning with Gardon et al. contributions [10-12]) were performed on heat/mass transfer using impinging jets, and an early observation has been made in [11] about the importance of jet turbulence in heat transfer processes. It was shown that some seemingly anomalous heat-transfer phenomena can be explained as effects of the turbulence occurring in jets. Turbulence is generated by the jet itself and by possible external disturbances and varies significantly with the nozzle shape, the upstream conditions and the position within the jet. One decade after the observation of Gardon and Akrifat [11], Popiel and Boguslawski [13] claimed that nozzle exit configuration is the most important factor affecting the heat/mass transfer which occurs in the neighbourhood of the stagnation point. Despite these first very significant indications,

*Corresponding Author: kodjovi.sodjavi@univ-lr.fr

there are only a few studies dedicated to heat/mass transfer enhancement using active [14-17] or passive jet control [18-21].
Lee et al. [18] showed that the peak of Nusselt number generated on a heated plate by an impinging turbulent elliptic jet with an aspect ratio of 2.14, and having an exit Reynolds numbers Re=5000, 10000 and 20000, is larger than that for its counterpart impinging circular jet. The authors speculated that this is due to the large entrainment rate and large scale coherent structures of the elliptic jet. For a nozzle-to-plate distance of 2 nozzle equivalent diameters (the equivalent diameter is based on the free area of the nozzle) and for Re=10000 or 20000, the Nusselt number of elliptic jet exhibited, beyond the main maxima, a second and third peaks. More recently the same authors [19] compared three round orifice nozzles with an exit Reynolds numbers in the range of 10000-30000 and a nozzle-to-plate spacing in the range 2–10 nozzle diameters. The orifices were square-edged, standard-edged and sharp-edged, respectively. The square-edged orifice is straight hole with straight-through edges (90° corners at the hole). The standard edged orifice has square edged corners at the entrance, and a bevel edges at the outlet. The sharp-edged orifice is bevelled through the entire thickness of the hole (with an angle of 45° relative to the axis normal to the orifice plate). In the stagnation region, the sharp-edged orifice jet yields significantly higher heat transfer rates than either the standard-edged orifice jet or square-edged orifice jet. The effect of nozzle exit configuration on the stagnation point heat transfer is more sensible at shorter nozzle-to-plate spacing.
Gulati et al. [22] have compared the local heat transfer distribution of jets issuing from circular, square and rectangular nozzles with an exit Reynolds numbers varied between 5000 and 15000 and a nozzle-to-plate spacing from 0.5 to 12 nozzle equivalent diameters. They found that, up to normalized nozzle-to-plate distance of 6, the Nusselt number corresponding to the rectangular jet was higher in the stagnation region than those of circular and square jets. For all three nozzle geometries, the heat transfer rate increased with increasing Reynolds number. The radial distribution of the local heat transfer exhibited two peaks for normalized nozzle-to-plate distance smaller than 4. It was also observed that, the location of the secondary peak was shifted towards the stagnation point with decreasing nozzle-to-plate distance.
Gao and Ewing [20] were the first authors which introduce passive control of impinging jet for heat transfer enhancement using vortex generators (triangular tabs). Heat transfer measurements were performed for impinging round pipe jets with a Reynolds number of 23000 and normalized nozzle-to plate distances ranging from 1 to 10. The authors found that the addition of triangular tabs at the pipe exit had a significant effect on the heat transfer produced by impinging jet. The local heat transfer enhancement was in excess of 25%. According to Lee et al [18], heat transfer enhancement in asymmetric jet is correlated to their entrainment rates. Lobed jets are known to increase significantly ambient fluid entrainment [8, 23-26], except when the lobed nozzle is a lobed straight tube [25].

The relation of the heat/mass transfer phenomenon with the large-scale structures which develop in the free jet region or with the subsequent flow dynamics in the stagnation and the wall jet regions is now recognized [27-30]. Therefore, the control of large-scale structures in impinging jets is a key element in the strategy of heat/mass transfer optimization. Passive control using undulated (or lobed) nozzle lip is particularly attractive because of easy implementation in industrial applications. Our previous investigations of the free lobed jets [25, 31-33], and the correlation suggested in the literature between the jet entrainment and the heat/mass transfer phenomenon when the jet impinges a wall, allow us to make right choices of lobed nozzle geometries to improve heat/mass transfer processes.

This paper presents the first results of an optimization approach of injection geometry, vis-à-vis the wall shear stress enhancement resulting from jet impingement. The jet injection is insured using a cross-shaped orifice perforated on either a flat or hemispherical surface.
It has already been shown in our previous investigation of impinging jet [34], that a jet issued from a cross-shaped orifice nozzle, increases significantly the wall shear rate on a flat plate, compared to a reference jet issued from a convergent nozzle. The hemispherical surface with a cross-shaped orifice considered in the present study is intended to increase the stretching of the shear-layer at the jet exit, aiming to generate efficient jet dynamics in terms of wall skin friction. To ensure continuity with the previous investigation [34], we choose similar jet Reynolds number equal to 5290, and we use the two already studied nozzles (convergent and cross-orifice on a flat plate), to which we add an innovative nozzle, i.e. the hemispherical cross-orifice nozzle. Contrary to previous investigation where the nozzle-to-wall distance was varied in the

range $2D_e$-$5D_e$, this distance is now kept constant, i.e. $H= 2D_e$ (with D_e = 7.8mm for each nozzle). This distance corresponds approximately to the first half of the potential core length of a round free jet [35]. The Kelvin-Helmholtz toroïdal vortices are well formed at this distance and are still well defined at the target wall. In the free lobed jet, vortex mechanisms are very complex since the nozzle exit [25, 26, 33, 36]. In such a jet, the core length is reduced but is still greater than $2D_e$. Thus with $H= 2D_e$, for all the jets considered, the wall is positioned inside the potential core region.

Wall shear rate distribution on the target plate is measured using electrodiffusion method, the same method as we have used before in [34]. Phares et al. [37] have made a critical survey of different techniques used for the measurements of wall shear stress and concluded that the electrodiffusion method provides the greatest accuracy of any indirect method. To our knowledge, Kataoka et al. [38] have been the first to introduce this technique for the measurement of wall skin friction generated by impinging jet. We used electrodiffusion method (ED) and the Particle Image Velocimetry (PIV) for measurements of wall shear rate and two velocity components, respectively. Both techniques are complementary as the PIV fails at the vicinity of the wall due to the laser scattering by the solid surface.

The paper is structured into two main Sections. In the Section 2 we outlined the employed procedures, and the Section 3 is dedicated to results analysis.

2. EXPERIMENTAL APPARATUS AND METHODS

2.1 Jet flow generation

The experiments are conducted in a liquid jet impinging orthogonally onto a wall. The schematic diagram of its generation in a reservoir is shown in Fig.1. A gear pump (Ismatec with a GJ-N23 head) draws its supply from a reservoir and delivers the fluid to a nozzle. The liquid jet issued from the nozzle impinges the circular target disc provided with six electrodes (Fig.2) which are the probes for electrodiffusion measurements (see section 2.3 below). The temperature of the fluid is controlled by a cooling coil within ±0.2°C. The nozzle is screwed to a 200 mm length stainless steel tube with inner and outer diameters of 15 and 20 mm, respectively. A honeycomb manufactured of a 7 mm thick disc by drilling 17 holes with a diameter of 2 mm was fitted in the tube inlet. The nozzle assembly was located in a support which allowed vertical movement for accurate alignment of the nozzle axis with the electrodes centre. The reservoir was placed on the sliding compound table (Proxxon KT 150) which allowed movement in the axial and transverse direction of the tube with a precision of 0.05 mm.

The target (Fig.2) was manufactured of a Poly(methyl methacrylate) disc with a diameter of 100 mm and a thickness of 17 mm by first drilling the holes to insert the electrodes. The platinum foil with a diameter of 50 mm and a thickness of 50 µm was assembled centrally with the disc using Neoprene glue. Holes with a diameter 0.7 mm were drilled through the platinum foil as a continuation of the holes in the disc. The electrodes were manufactured of a 0.5 mm platinum wire which was coated electrophoretically using a deposit of a polymeric paint. After soldering the connecting cables, the electrodes were glued with an epoxy resin into the disc, so that the tops of the platinum wires just projected above the platinum foil. The wires were then rubbed down flush with the surface of the platinum foil using progressively finer grades of emery paper. The last emery paper had a grit size of 10 µm. The whole surface was then polished using a fine dental paste. The resulting surface roughness was about 0.11 µm which is much less than the Nernst diffusion layer thickness estimated at 10 µm. The test fluid was a 20 mol/m^3 equimolar potassium ferri/ferrocyanide aqueous solution with 1.5 % mass K_2SO_4 as supporting electrolyte. The density of the solution was 1.007×10^3 kg/m^3, its kinematic viscosity 1.065×10^{-6} m^2/s and its diffusivity 7.5×10^{-10} m^2/s at 20 °C. The resulting Schmidt number (Sc) was 1.420×10^3. The number (n) of electrons involved in the electrochemical reaction was equal to 1.

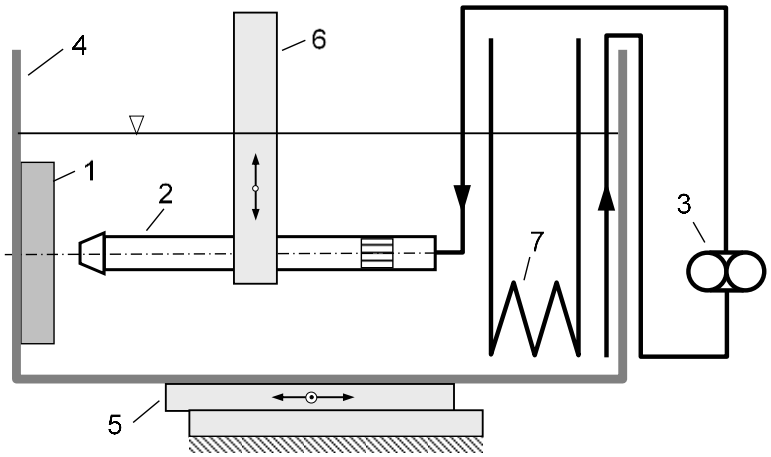

Fig. 1 Diagram of apparatus: 1 target disc with electrodes, 2 tube with nozzle and honeycomb, 3 pump, 4 reservoir, 5 compound table, 6 nozzle holder, 7 cooling coil

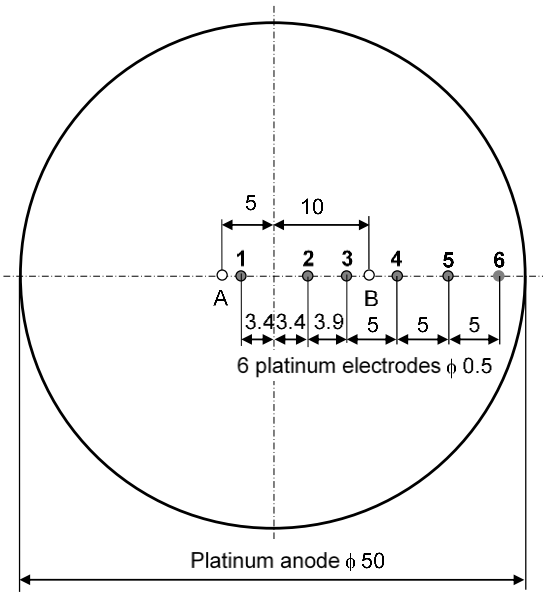

Fig. 2 Target disc with electrodes: 1-6 electrodes, A, B limits of stagnation point displacement

In this study, two cruciform orifice jets were compared to the reference convergent jet. The convergent nozzle (designated by CONV) had an exit plane diameter of 7.8 mm with an area contraction 4:1 on a length of 17 mm. Its sketch and others details of the experiment setup can be found in Kristiawan et al. [34] and Meslem et al. [39]. Schematics of the two cruciform nozzles are shown in Fig. 3. They are given by the projection of plane cruciform orifice (Fig.3 b) onto a plane surface (Cruciform Orifice made on a flat Plate, CO/P, see Fig.3 a) and onto a spherical surface (Cruciform Orifice made on a Hemisphere, CO/H, see Fig.3 c and d). The two lobed nozzles had a same equivalent diameter D_e = 7.8 mm. The Reynolds number based on D_e and the jet bulk-velocity ($W_b = 4Q_0/\pi D_e^2$) is Re_b = 5290. The distance H between the jet exit and the target wall is kept constant ($H = 2D_e$) for all the measurements. The coordinate system (r,Y,Z) attached to the nozzle is shown in Fig.4. As sketched, the flow field may be divided into several regions. In the neighborhood of the stagnation point S, the flow spreads in radial directions parallel to the wall. The development of the impinging jet flow field near the wall is typically divided in two regions: the stagnation region associated with the turning of the mean flow, $r/D_e<1$, and the radial wall jet region, $r/D_e>1$.

2.1 PIV measurements

We investigated the flow field by 2D2C PIV (two in-plane velocity components in a plane field). The experiments were carried out with a Quantel BigSky 200 mJ dual Yag laser and a FlowSense EO (CCD) camera of 2048×2048 pixels resolution with a pixel size of 7.4×7.4 μm^2. The total field of view is about $2D_e$×$6D_e$ to cover free and wall jet regions (Fig. 4). The light sheet optics produces a laser sheet of less than 1 mm in thickness. The maximum acquisition frequency of the PIV system is 15 Hz.

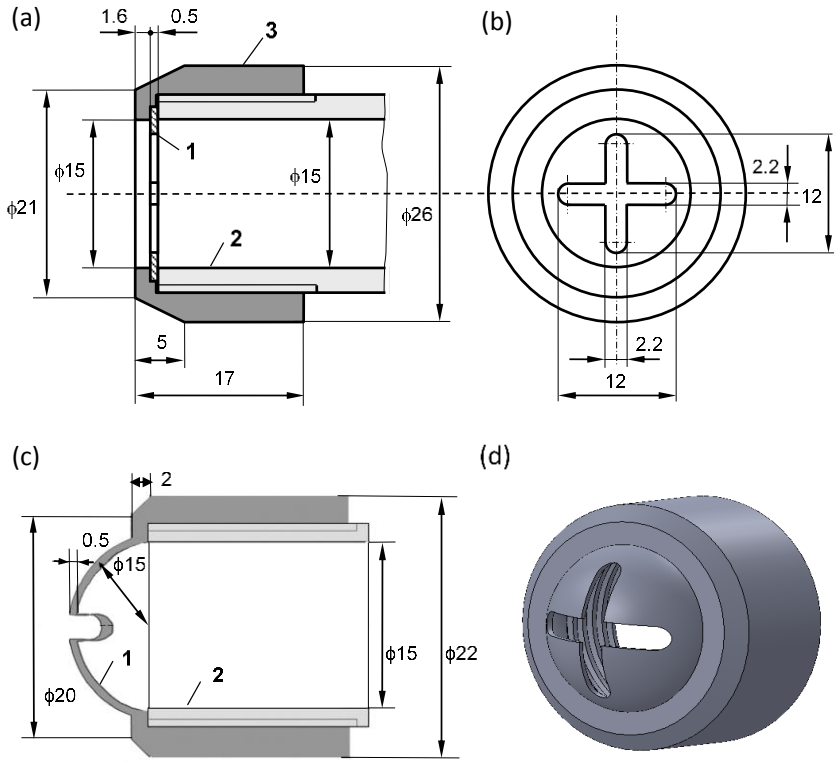

Fig. 3 Sketch of nozzles: (a and b) Cross-Orifice on Plane (CO/P); (c and d) Cross-Orifice on Hemisphere (CO/H). 1 – surface supporting the cross orifice, 2 – tube, 3 – sleeve nut

For each experiment, 500 couples of images were acquired. The recordings were analyzed through two different windows. The velocity distribution in the total field of view ($2D_e$×$6D_e$) was calculated using an adaptive multi-grid correlation algorithm handling the window distortion and the sub-pixel window displacement (128×128, 64×64, and 32×32 pixels) and 50% overlapping. To get more velocity vectors in the radial wall jet region (Fig. 4) the same algorithm was used with a final grid composed of 8×64 pixels interrogation windows and 50 % overlapping. The prediction-correction validation method of multi-grid algorithm identified on average less than 1% erroneous velocity vectors, which are replaced using a bilinear interpolation scheme. For all the experiments, the uncertainty of the measurement due to the displacement error was estimated to be in the range of 1 to 3 % outside the boundary layer. The uncertainty rises near the impinging plate due to laser scattering, so that the boundary layer is not accessible using PIV technique. This difficulty is bypassed thanks to another measurement technique which is the electrodiffusion method described in the next section.

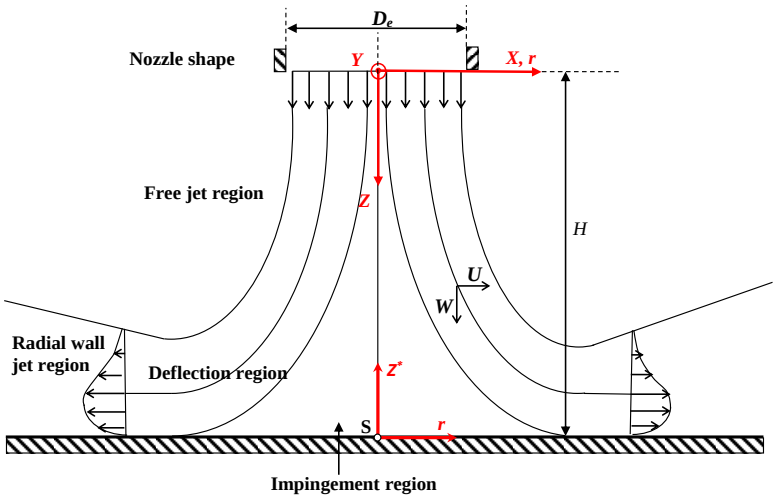

Fig. 4: Schematic description of impinging jet on a flat plate and associated system coordinates

2.1 Electrodiffusion measurements

The electrodiffusion method for wall shear rate measurement uses a working electrode flush-mounted on the wall which measures limiting diffusion current. This technique was extensively described in Kristiawan et al. [34], El Hassan et al. [27] and Meslem et al. [39], thus, only a brief summary will be given here. This technique has been developed for measuring the average rates of mass transfer and their fluctuations on a wall.

The method is based on electrochemical redox reaction whose rate is very fast but the electric current is limited by convective mass transfer into the measuring electrode (probe). For the total current through a circular electrode in a viscosimetric flow with uniform wall-shear rate, the formula corresponding to the Leveque's equivalent equation for heat transfer was established in Reiss et al. [40] and is given by:

$$I_L = \frac{0.884\pi}{3^{1/3}\,\Gamma(4/3)}\, n\,F\,C\,\gamma^{1/3}\,D_C^{\,2/3}\,R^{5/3} \tag{1}$$

Where C is the bulk concentration, D_C the diffusion coefficient of active species, F the Faraday constant, n the number of electrons taking part in the electochemical reaction, R the radius of the electrode and Γ the gamma function.

Let us recall that the basic assumptions for the derivation of the Leveque relationship (Eq.1) is that the probe is in a flow with parallel streamlines and uniform wall-shear rate γ. In the case of impinging jet, the streamlines in the wall vicinity spread radially from the stagnation point and the wall-shear rate increases with r. Kristiawan et al. [34] have determined the drawbacks of application of this equation in the stagnation region for an electrode with R = 0.25 mm. At a radial distance r = 1mm from the stagnation point, the authors have found 2.1% error in wall shear rate. Taking into account the others parameters which can affect the wall shear rate, Meslem et al. [39] conclude that the error on the wall shear rate using Eq.1 is less than 5% for $r/R \geq 4$.

3. RESULTS AND DISCUSSION

3.1 Flow characteristics

In Fig.5, spatial developments of the two cruciform jets (CO/P and CO/H) in their respective major plane (MP) and minor plane (mP) are compared to the development of convergent jet (CONV) in its longitudinal plane. For highlighting recirculation regions if any, streamlines are superimposed to the mean vector field. When one compares all the fields, an atypical behavior appears in the mP of CO/H nozzle jet: a large recirculation zone is visible in the deflection region on the both sides of the jet-axis. Also, the spreading of the wall jet in mP is very large compared to the MP of the same jet.
The Fig. 6 allows quantifying jet expansion using the jet width in its free region. In each cruciform jet, the jet width is given in mP and MP, respectively. Whereas in CO/P case, the jet tends to become circular, in CO/H case the jet remains more expanded in MP than in mP.

As was emphasized by Nastase et al. [41], the major difference between flat and hemispherical lobed orifice flows is given by the position of the development of secondary streamwise structures. In a flat lobed orifice, streamwise vortices develop in the lobe troughs leading to axis-switching phenomenon (Fig. 5 b and Fig. 6 a). In a hemispherical lobed orifice, the curvature of the surface containing a lobed orifice completely changes the behavior of the generated jet flow. As visible in Fig. 5 c and Fig. 6 b, no axis-switching occurs: the jet conserves the shape imposed initially by the nozzle with the major and the minor axis oriented in the same way as those of the nozzle. In this jet, the development of streamwise secondary vortices occurs on the top of each lobe [41].

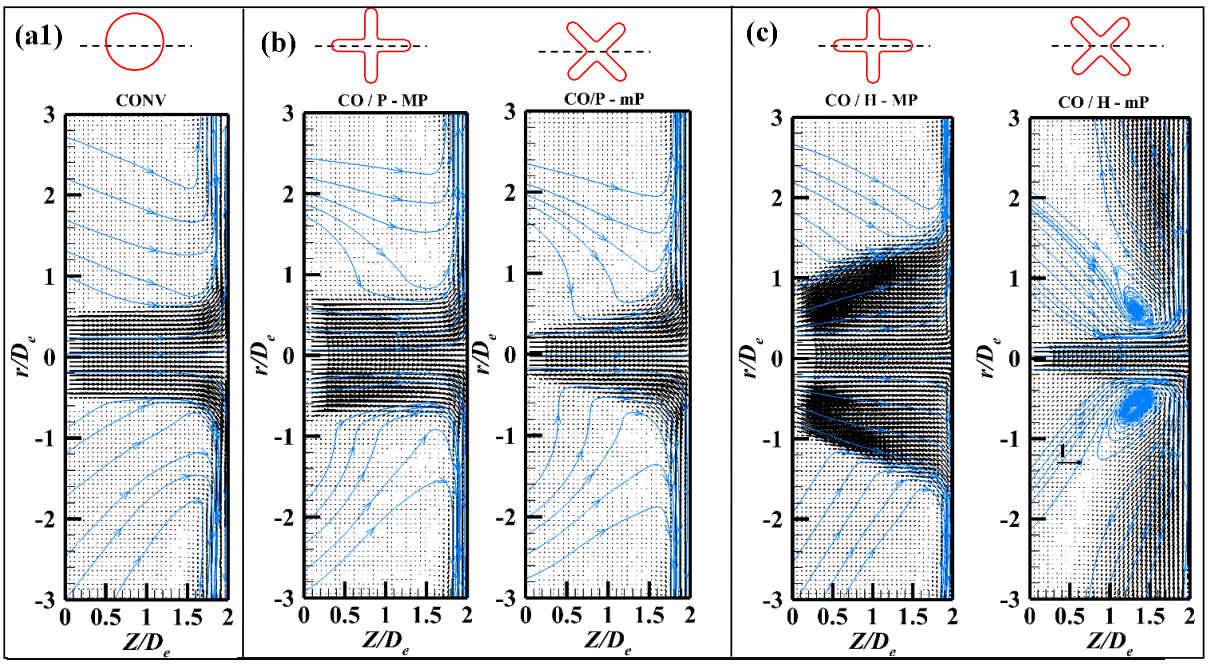

Fig.5 Mean vector fields $\left(\frac{W}{W_0}\vec{e}_z + \frac{U_r}{W_0}\vec{e}_r\right)$ and the corresponding streamlines (in blue color): convergent nozzle (a), cross-shaped orifice on plane (b), cross-shaped orifice on hemisphere (c)

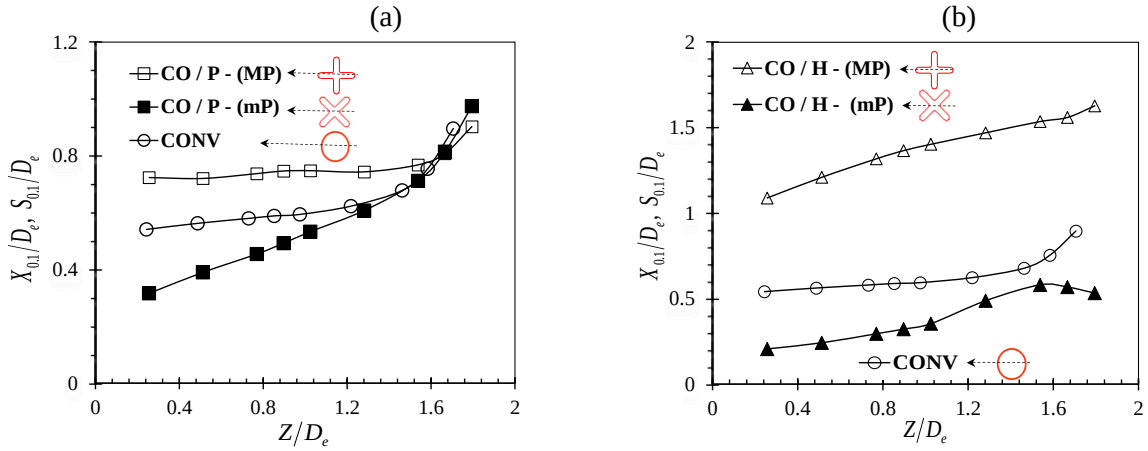

Fig.6 Jet widths in the free jet region of cruciform jet: (a) Cross Orifice on Plane CO/P; (b) Cross Orifice on Hemisphere CO/H– comparison to the convergent jet

In order to characterize the imprint of nozzle geometry on jet inlet conditions, the radial distributions of mean streamwise velocity and, streamwise and spanwise turbulence intensity are extracted from PIV fields (Fig. 5) and are given in Fig. 7. The axial position $Z = 0.25D_e$ is chosen to define jet inlet conditions. Because of laser scattering which occurs on the nozzle surface, measurements upstream that location are subjected to large uncertainties.

Owing to the flow symmetry in each plane, only half-profiles are plotted. The shapes of theses profiles (Fig.7) are linked to the exit nozzle geometry. The mean streamwise profile of convergent jet is flat while for cruciform nozzles a two-step distribution characterizes the major plane. The same behavior was also observed by Nastase et al. [42] in a jet from a flat cross-shaped orifice and by Hu et al. [43] in a six-lobed pipe jet. In the lobed jets, the major plane presents two shear layers: the inner shear layer between lobes and jet central core, and the outer shear layer at the interface with ambient fluid. In the minor plane, the mean velocity profile is similar to that of convergent nozzle but with smaller diameter. The corresponding streamwise turbulent intensity profiles (Fig.7 b) exhibit very low values (2%) at the jet center, and sharp peaks in the shear layers. Due to the presence of two shear layers (inner and outer) in the major plane, there are two peaks in the corresponding streamwise turbulence profiles. Whether for the jet issuing from the CO/P or CO/H nozzles, a wide region of intensive mixing characterized by a high turbulent intensity (up to 40% of W_0) can be observed. Similar streamwise turbulence profiles were measured by Hu et al. [43] in their six-lobed jet.

Table 1: Experimental initial conditions of the three studied flows

N	***Symbol***		$W_o = W(Z=0.25D_e)$ (m/s)	W_o/W_b	δ_o^*/D_e	θ_o/D_e	$H^* = \delta_o^*/\theta_o$
CONV			0.817	1.18	0.059	0.022	2.68
C O / P	**(MP)**		1.20	1.66	0.068	0.025	2.73
	(mP)		1.20	1.66	0.061	0.022	2.73
C O / H	**(MP)**		1.45	2.11	0.153	0.055	2.79
	(mP)		1.45	2.11	0.043	0.016	2.69

N: Nozzle; CONV: Convergent; CO/P: Cross-shaped Orifice on Plane; CO/H Cross-shaped Orifice on Hemisphere; MP: Major Plane; mP: minor Plane

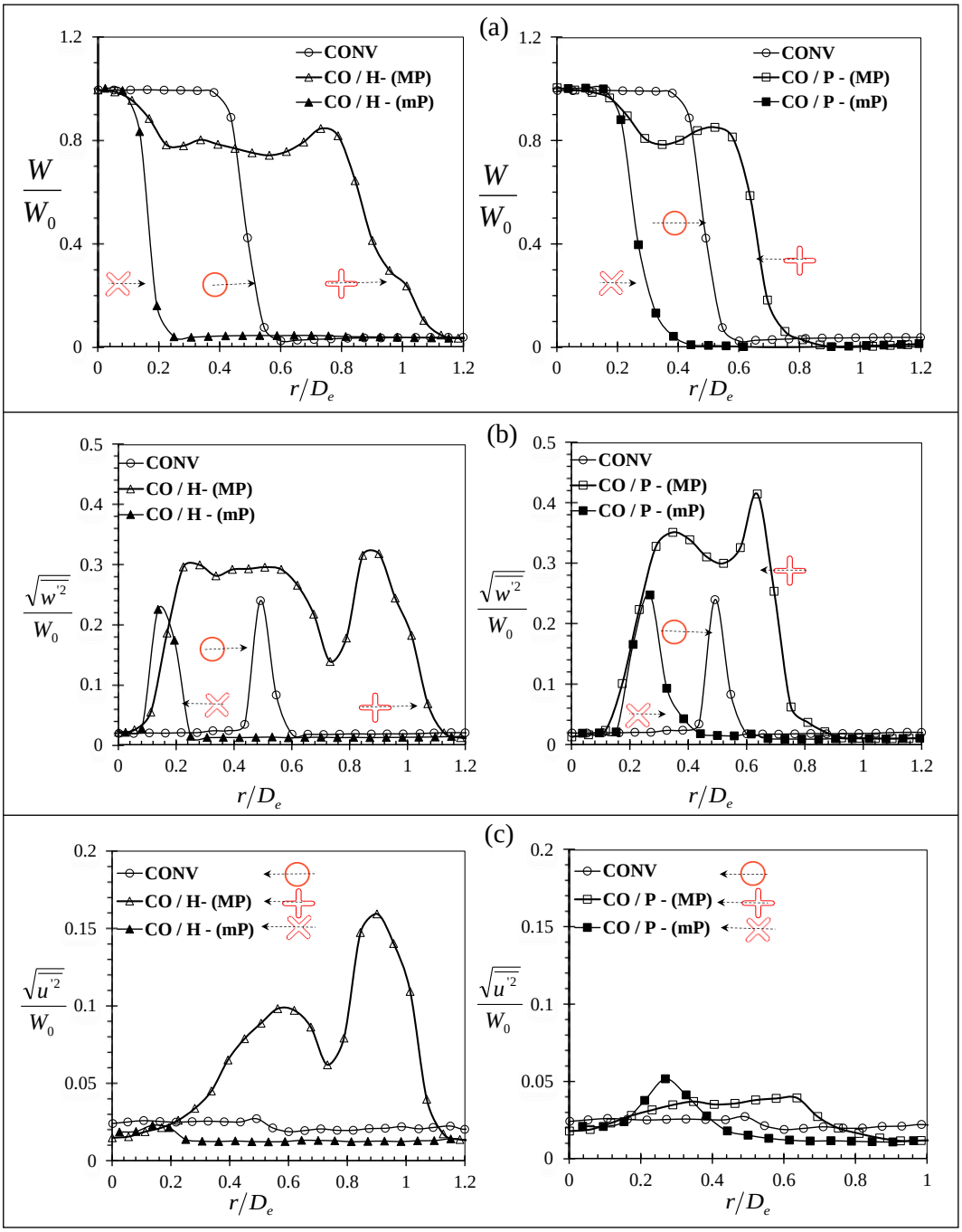

Fig.7 Radial distribution at the jet exit Z=0.25D_e of the mean axial velocity W (a), of the rms axial velocity $\sqrt{w'^2}/W_0$ (b), and of the rms radial velocity $\sqrt{u'^2}/W_0$ (c)

The spanwise turbulent intensity distribution (Fig. 7 c) for the convergent nozzle has low uniform values across the jet as expected. The spanwise turbulent intensity distribution in CO/P nozzle jet also exhibits low values. The peak in spanwise turbulent intensity visible around r = 0.3D_e in mP of this jet corresponds to the development of secondary vortices in the lobe trough [42]. In the mP of CO/H nozzle jet, the spanwise turbulent intensity is low and no peak is present on the distribution because no streamwise vortices develop there. In MP of CO/H jet, spanwise turbulent distribution is atypical with very high levels due to flow stretching generated by the curvature of the nozzle (see Fig. 5 c, LHS). The particular distribution of spanwise turbulent intensity at the exit of each lobed jet is linked to the development of their respective

streamwise vortices. In the CO/P nozzle jet, streamwise structures develop in the lobe troughs, whereas in the CO/H nozzle jet, streamwise vortices appear on the top of the lobe [41].

Details about initial momentum thickness and outlet velocity are summarized in Table 1. The momentum thickness for the jet issuing from CONV and CO/P nozzles in non-dimensional form θ_0/D_e ranges from 0.022 to 0.026. These values falls in the range reported in the literature [23]. For the jet issuing from CO/H nozzle, θ_0/D_e takes a common value in the minor plane mP, whereas in the major plane MP its value (0.055) it out of the usual range, due to flow stretching in this plane.

Considering all three jets of the present investigation, the axial turbulence intensity has a low value around 2% (Fig. 8 a) as previously noted on the corresponding exit turbulence profiles (Fig. 7 b). As the impingement plate is approached, the turbulence intensity increases and our results for the reference round jet are in a good agreement with those of Baydar and Ozmen [44]. However, the turbulence intensity of cruciform nozzle jets exhibit marked difference compared to that of the convergent jet. In the CO/P nozzle jet, two peaks are identified on the axial fluctuation. Whereas the second peak near the target is believed to be related to the wall damping effect [45], the occurrence of the first peak is not fully understood. From Zaman et al. [46] study of a free rectangular lobed jet, the appearance of a sharp peak on the axial turbulence intensity near the jet exit is expected to be related to the merging of the shear layers shed from an individual lobe. The authors observed in fact that the distance Z of the location of the first peak scales on the width of the lobes (a_l), i.e. $4 \leq Z/a_l \leq 6$. We have found in our case a value of 5.2 which is consistent with the values reported in [46].
In the CO/H nozzle jet, no peak is visible on the axial fluctuation (Fig. 8 a) which increases monotonically from $Z = 0.4D_e$ towards the wall, with a level being two times higher in average than that of CO/P nozzle jet. The high level of jet centerline fluctuations in CO/H nozzle jet is probably related to flow agitation by the numerous vortices generated in this jet (see Fig. 8 b) that deeply penetrate the jet core. This particular behavior is undoubtedly related to the hemispherical geometry which introduces supplementary shear to the one originating from the corrugated nozzle lip.

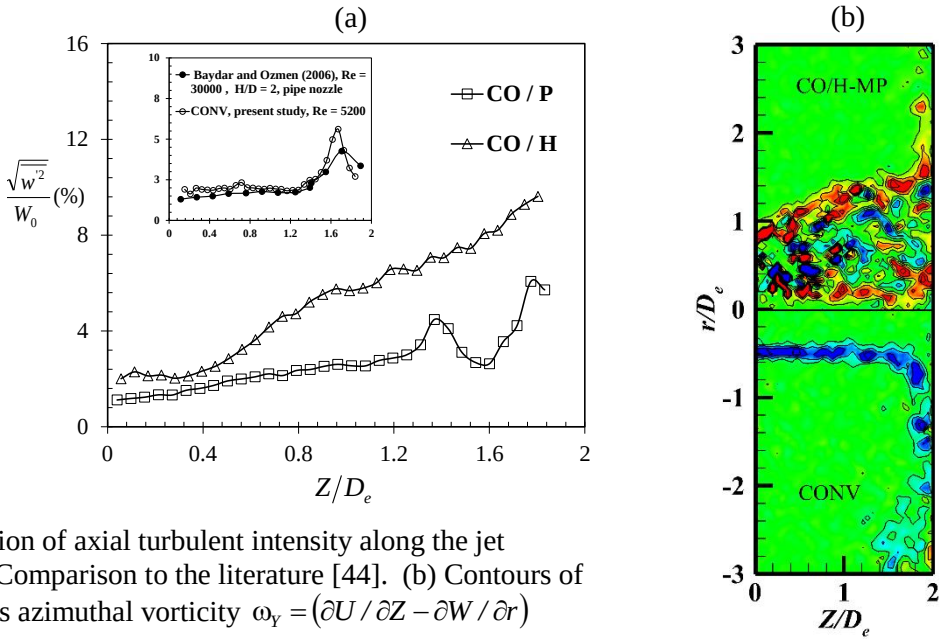

Fig.8 (a) Distribution of axial turbulent intensity along the jet centerline – Comparison to the literature [44]. (b) Contours of Instantaneous azimuthal vorticity $\omega_Y = (\partial U/\partial Z - \partial W/\partial r)$

3.1 Wall shear rates

Local and instantaneous shear rate at the very vicinity of the wall and perpendicular to the impinging jet was acquired using the electrodiffusion method described above in paragraph 2.3. To measure the mean and the rms values of the wall shear rate, the signals were recorded with a sampling frequency of 500Hz on a period of 40 sec.
Radial distributions of the wall shear rate were obtained by moving the stagnation point horizontally in the range limited by the points A and B on the target shown in Fig. 2. Thereby, several values of the wall shear rate measured by different electrodes at similar radial distances from the stagnation point were obtained. Based on the comparison of the measured values for a given radial position, it was observed that the repeatability is insured with maximum deviation of ±5% of the mean value. Knowing the complexity of the lobed jets, thirty-one displacements of the stagnation point with a step of 0.5 mm were performed to well capture the details of wall shear rate profiles, except for convergent nozzle jet and for the minor plane of CO/H nozzle jet, for which sixteen displacements were sufficient with a step of 1 mm.

The radial distributions of the mean wall-shear rate of the cruciform nozzle jets are compared to that of convergent nozzle jet in Fig. 9. In both CO/P and CONV cases, the value of wall shear rate is almost zero at the stagnation point, whereas its value is relatively high in CO/H case. Recall here that in the jet from CO/H nozzle, centerline streamwise turbulence intensity does not start to decrease as in CO/P and CONV jets at the vicinity of the stagnation point (Fig. 8 a). The strong stretching of the flow by CO/H nozzle and the resulting deep penetration of the vortices towards the jet axis (Fig. 8 b) are responsible of high turbulence (Fig. 8 a) and high wall shear rate (Fig. 9 a2) in the corresponding stagnation region.

In each jet, with increasing radial distance the wall shear rate increases monotonically, reaches its maximum, and then decreases. The maximum is located around r/D_e = 0.68 for the convergent jet, at r/D_e = 0.58 and r/D_e = 0.53 in the MP and mP, respectively of CO/P nozzle jet, and *at* r/D_e = 0.19 in both major and minor planes of CO/H nozzle jet.

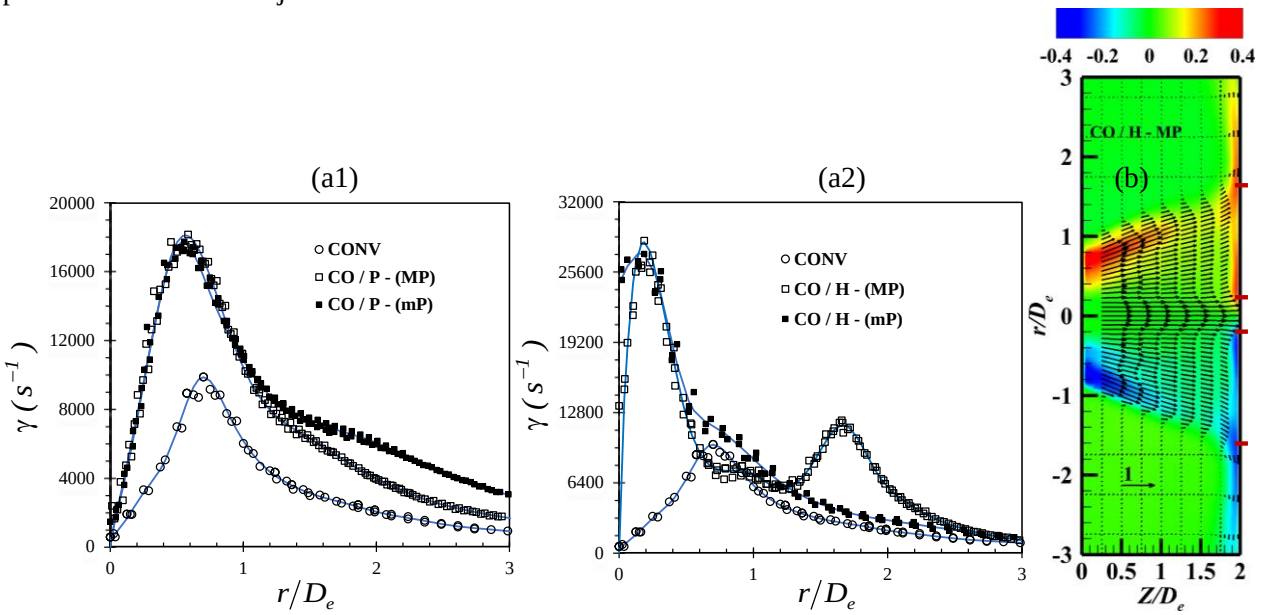

Fig.9 (a) Mean wall shear rate as a function of radial distance from stagnation point: (a1) CONV and CO/P nozzles; (a2) CONV and CO/H nozzles - the solid lines are the best fit curves of experimental data. (b) Vector field $\left(\frac{W}{W_0}\vec{e_z}+\frac{U}{W_0}\vec{e_r}\right)$ and radial velocity U/W_0 contours (colormap) in the MP of CO/H nozzle jet. The red ticks indicate the positions of maximum wall shear rate γ_{max}

Note that in the major plane MP of CO/H nozzle jet (Fig. 9 a2) a secondary peak appears around $r/D_e = 1.64$ due to the impingement of the outer sub-layer (see Fig. 9 b). In Fig. 9 b, peak locations are indicated by red ticks. The maximum value of wall shear rate (Fig. 9 a1 and a2) is around 9880 s^{-1}, 18360 s^{-1} and 28000 s^{-1} for the CONV, CO/P and CO/H nozzle jets, respectively. For the same exit bulk-velocity W_b, the maximum wall shear rate in CO/P and CO/H nozzle jets are almost two and three times respectively higher than the one of the reference convergent jet. Hence, CO/H nozzle jet is an excellent candidate in passive strategies to enhance local heat and mass transfer in industrial applications. Indeed, the transfer mechanisms of heat and mass between the jet and the target wall are closely linked to the wall shear rate level.

4. CONCLUSIONS

The present study examines the relation between nozzle geometry and wall shear stress generated by a jet impinging orthogonally on a flat plate. Electrodiffusion and Particle Image Velocimetry measurements were carried out using three nozzle geometries. Two cruciform jets, one issuing from a plane orifice nozzle (CO/P) and the second one from a hemispherical orifice nozzle (CO/H), were compared to a reference round jet issuing from a convergent nozzle. The Reynolds number, based on nozzle's equivalent diameter and on the exit bulk-velocity, was equal to 5290 in each flow. For the same exit bulk-velocity, the maximum wall shear rate in CO/P and CO/H nozzle jets are almost two and three times respectively higher than the one of the reference convergent jet. These results highlight the fact that the impinging flow dynamics near the wall is affected by the nozzle exit. The CO/H nozzle jet is characterized by a wide region of intensive mixing and a high turbulent intensity in its free jet region, undoubtedly at the origin of high friction levels. Therefore, the CO/H nozzle jet is an excellent candidate in passive strategies to enhance local heat and mass transfer in industrial applications.

NOMENCLATURE

A_0	Free nozzle area	(m^2)	U	radial velocity	(m/s)
C	concentration of of depolarizer in bulk	(mol m^{-3})	W	streamwise velocity	(m/s)
D_C	diffusion coefficient of depolarizer	(m^2 s^{-1})	(X, Y, Z)	system of coordinates attached to the nozzle	(m)
D_e	nozzle equivalent diameter $D_e = (4A_0/\pi)^{0.5}$	(m)	$X_{0.1}$	radial distance at the periphery of the potential core where $W(X_{0.1}) = 0.1\ W_C$, in major plane	(m)
F	Faraday constant (96485 $Cmol^{-1}$)		$S_{0.1}$	radial distance at the periphery of the potential core where $W(S_{0.1}) = 0.1\ W_C$, in minor plane	(m)
H	nozzle-to-plate axial distance	(m)	γ	wall shear rate	(s^{-1})
I	limiting diffusion current diffusion current	(A)	**Subscripts**		
Nu	Nusselt number, $Nu = h\ D\ /\ \lambda$		L	Lévêque equation	
n	the number of electrons taking part in the electrochemical reaction		0	jet exit value at the center of the nozzle and at $Z = 0.25D_e$	
Q	volumetric flow rate	(m^3/s)	C	jet centerline value	
R	radius of electrode	(m)			
r	radial distance measured from stagnation point	(m)			
Re	Reynolds number, $W_0D_e\ /\ \nu$				

REFERENCES

[1] Xu, G. and Antonia, R.A., "Effect of different initial conditions on a turbulent round free jet," Experiments in Fluids, **33**, p p. 677–683, (2002).

[2] Quinn, W.R., "Upstream nozzle shaping effects on near field flow in round turbulent free jet," European Journal of Mechanics B-Fluids," **25**, pp. 279-301, (2006).

[3] Husain, Z.D. and Hussain, A.K.M.F., "Axisymetric Mixing Layer: Influence of the Initial and Boundary Conditions," AIAA Journal, **17**(1): pp. 48-55, (1979).

[4] Nathan, G.J., Mi, J., Alwahabi, Z.T., Newbold, G.J.R., Nobes, D.S. "Impacts of a jet's exit flow pattern on mixing and combustion performance". Progress in Energy and Combustion Science, **32**(5-6): pp. 496-538 (2006).

[5] Hussain, A.K.M.F. and Zaman K.B.M.Q., "The 'preferred mode' of the axisymetric jet," Journal of Fluid Mechanics, **110**: p. 39-71, (1981).

[6] Hussain, F. and Husain, H.S., "Elliptic jets. Part1. Characteristics of unexcited and excited jets," Journal of Fluid Mechanics, **208**:p p. 257-320, (1989).

[7] Zaman, K.B.M.Q., Reeder, M.F., and Samimy M., "Control of axisymmetric jet using vortex generators," Physics of Fluids, **6**(2): pp. 778-793, (1994).

[8] Gutmark, E.J. and Grinstein, F.F., "Flow Control with Noncircular Jets," Annual Reviews of Fluid Mechanics,. **31**: pp. 239-272, (1999).

[9] Mi, J. and Nathan, G.J., "Effect of small vortex-generators on scalar mixing in the developing region of a turbulent jet," international Journal of Heat and Mass Transfer, **42**: pp. 3919 -3926, (1999).

[10] Gardon, R., "Heat Transfer Between a Flat Plate and Jets of Air Impinging on It," Int. Dev. Heat Transfer (ASME), pp. 454-460, (1962).

[11] Gardon, R. and Akfirat , J.C., "The role of turbulence in determining the heat-transfer characteristics of impinging jets," International Journal of Heat and Mass Transfer, **8**: pp. 1261-1272, (1965).

[12] Gardon, R. and Akfirat, J.C., Closure to "Discussion of 'Heat Transfer Characteristics of Impinging Two-Dimensional Air Jets," (1966, ASME J. Heat Transfer, 88, pp. 107–108). Journal of Heat Transfer, **88**(1): pp. 108-108, (1966).

[13] Popiel, C.O. and Boguslawski, L., "Effect of Flow Structure on the heat or mass tansfer on a Flat plate in Impinging Round jet," in 2nd UK National Conf. on Heat Transfer, (1988).

[14] Vejrazka, J. Tihon, J., Marty, Ph., Sobolík, V.," Effect of an external excitation on the flow structure in a circular impinging Jet," Physics of Fluids (1994-present),. **17**(10): pp. 105102.1-105102.4 (2005).

[15] Alekseenko, S.V., Bilsky, A.V., Dulin, V. M. and Markovich, D. M. ., "Experimental study of an impinging jet with different swirl rates," International Journal of Heat and Fluid Flow, **28**(6):p p. 1340-1359, (2007).

[16] Roux, S., Fenot, M. Lalizel, G., Brizzi, L.E., Dorignac, E.,"Experimental investigation of the flow and heat transfer of an impinging jet under acoustic excitation," International Journal of Heat and Mass Transfer, **54**: pp. 3277–3290, (2011).

[17] Trávníček, Z. Němcová, L., Kordík, J., Tesař, V. and Kopecký, V., "Axisymmetric impinging jet excited by a synthetic jet system," International Journal of Heat and Mass Transfer, **55**(4): pp. 1279-1290 (2012).

[18] Lee, S.-J., Lee, J.-H., and Lee, D.-H., "Local heat transfer measurements from an elliptic jet impinging on a flat plate using liquid crystal," International Journal of Heat and Fluid Flow **37** .pp. 967-976 (1994).

[19] Lee, J. and Lee, S.J., "The effect of nozzle configuration on stagnation region heat transfer enhancement of axisymmetric jet impingement," international Journal of Heat and Mass Transfer, **43**: pp. 3497-3509, (2000).

[20] Gao, N., Sun, H., and Ewing, D., "Heat transfer to impinging round jets with triangular tabs," International Journal of Heat and Mass Transfer, **46**(14): pp. 2557-2569, (2003).

[21] Nakod, P.M., Prabhu S.V., and Vedula, R.P., "Heat transfer augmentation between impinging circular air jet and flat plate using finned surfaces and vortex generators," Experimental Thermal and Fluid Science, **32**(5): pp. 1168-1187, (2008).

[22] Gulati, P., Katt, V., and Prabhu S.V., "Influence of the shape of the nozzle on local heat transfer distribution between smooth flat surface and impinging air jet," International Journal of Thermal Sciences, **48**: pp. 602–617 (2009).

[23] Gutmark, E.J. and Ho, C.M., "Preferred modes and the spreading rates of jets," Physics of Fluids, **26**(10): pp. 2932–2938, (1983).

[24] Zaman, K.B.M.Q., "Spreading characteristics and thrust of jets from asymmetric nozzles," AIAA Paper No 96-0200, (1996).

[25] Nastase, I. and Meslem, A., "Vortex dynamics and mass entrainment in turbulent lobed jets with and without lobe deflection angles," Experiments in Fluids, **48**(4): pp. 693-714, (2010).

[26] Hu, H., Kobayashi, T., Saga, T., Sagawa S. and Taniguchi, N., "Particle Image Velocimetry and Planar Laser Induced Fluorescence Measurements on Lobed Jet Mixing Flows," Experiments in Fluids (Suppl.), pp. S141-S157, (2000).

[27] El-Hassan, M., Hassan, A., H., Sobolik, V., Vétel, J., Abed-Meraim, K., Garon, A., Sakout, A. "Experimental investigation of the wall shear stress and the vortex dynamics in a circular impinging jet," Experiments in Fluids, **52**(6): pp. 1475-1489, (2012).

[28] Violato, D. Ianiro, A., Cardone, G., Scarano, F., "Three-dimensional vortex dynamics and convective heat transfer in circular and chevron impinging jets," International Journal of Heat and Fluid Flow, **37**: pp. 22–36, (2012).

*Corresponding Author: f.author@affiliation.com

[29] Hadziabdic, M. and Hanjalic, K., "Vortical structures and heat transfer in a round impinging jet," Journal of Fluid Mechanics, **596**: pp. 221-260, (2008).
[30] Hall, J.W. and Ewing, D., "On the dynamics of the large-scale structures in round impinging jets," Journal of Fluid Mechanics, **555**: pp. 439-458, (2006).
[31] Nastase, I. and Meslem,A., "Passive control of jet flows using lobed nozzle geometries," Mécanique et Industries, **8**: pp. 101-109, (2007).
[32] Nastase, I. and Meslem, A.,"Vortex dynamics and entrainment mechanisms in lobed jets," Bulletin of the American Physical Society, **52 (12)**, (2007).
[33] El-Hassan, M. and Meslem, A., "Time-resolved stereoscopic PIV investigation of the entrainement in the near-field of circular and daisy-shaped orifice jets," Physics of Fluids, **22**(035107), pp. -, (2010).
[34] Kristiawan, M., Meslem A., Nastase I. Sobolik, V., "Wall shear rates and mass transfer in impinging jets: Comparison of circular convergent and cross-shaped orifice nozzles," International Journal of Heat and Mass Transfer, **55**: pp. 282–293., (2012)
[35] Rajaratnam, N., Turbulent jets. 1976, Amsterdam, Netherlands: Elsevier Scientific Publishing Company.
[36] Belovich, V.M. and Samimy, M., "Mixing processes in a coaxial geometry with a central lobed mixer-nozzle," AIAA Journal, **35**(5), (1997).
[37] Phares, D.J., Smedley,G.T., and Flagan, R.C. , "The wall shear stress produced by the normal impingement of a jet on a flat surface," Journal of Fluid Mechanics, **418**: pp. 351-375, (2000).
[38] Kataoka, K. and Mizushina, T.," Local enhancement of the rate of heat-transfer in an impinging round jet by free-stream Turbulence," in Heat transfer 1974; Proceedings of the Fifth International Conference, Tokyo, Volume 2, Tokyo, (1974).
[39] Meslem, A. Sobolik, V., Bode, F., Sodjavi, K., Zaouali, Y., Nastase, I., Croitoru, C.,"Flow dynamics and mass transfer in impinging circular jet at low Reynolds number. Comparison of convergent and orifice nozzles," International Journal of Heat and Mass Transfer, **67**(0): pp. 25-45, (2013).
[40] Reiss, L.P. and Hanratty, T.J., "Measurement of instantaneous rates of mass transfer to a small sink on a wall," AIChE Journal, **8**(2): p. 245-247, (1962).
[41] Nastase, I., Meslem, A., and El-Hassan, M., "Image processing analysis of vortex dynamics of lobed jets from three-dimensional diffusers," Fluid Dynamics Research, **43**(6): pp. 065502, (2011).
[42] Nastase, I., Meslem, A. and Gervais, P. , "Primary and secondary vortical structures contribution in the entrainement of low Reynolds number jet flows," Experiments in Fluids, **44**(6): pp. 1027-1033, (2008).
[43] Hu, H., Saga, T., Kobayashi, T., Taniguchi, N., "Research on the Vortical and Turbulent Structures in the Lobed jet Flow Using Laser Induced Fluorescence and Particle Image Velocimetry Techniques," Measurement Science and Technology,. **11**: pp. 698-711, (2000).
[44] Baydar, E. and Ozmen Y., "An experimental investigation on flow structures of confined and unconfined impinging air jets," Heat and mass transfer, **42**(4): pp. 338-346, (2006).
[45] Cooper, D., Jackson, D. C., Launder, B. E., Liao, G. X.,"Impinging jet studies for turbulence model assessment—I. Flow-field experiments," International Journal of Heat and Mass Transfer, **36**(10): pp. 2675-2684, (1993).
[46] Zaman, K.B.M.Q, Wang, F.Y., Georgiadis, N.J., "Noise, Turbulence and Thrust of Subsonic Free Jets from Lobed Nozzles," AIAA Journal,. **41**(3). pp. 398-407, (2003)